Journal of Theoretical Biology 408 (2016) 155–166

Contents lists available at ScienceDirect

Journal of Theoretical Biology

journal homepage: www.elsevier.com/locate/yjtbi

Conformal growth of *Arabidopsis* leaves

Graeme Mitchison

Sainsbury Laboratory, Cambridge University, Cambridge, UK

HIGHLIGHTS

- The growth of Arabidopsis leaves follows a conformal map.
- A general mechanism that ensures at growth in plant leaves.
- An underlying linear gradient of growth rate in Arabidopsis leaves.
- Using complex numbers to model leaf growth.

ARTICLE INFO

Article history:
Received 21 April 2016
Received in revised form
7 July 2016
Accepted 14 August 2016
Available online 16 August 2016

MSC:
00-01
99-00

Keywords:
Leaf growth
Conformal map
Möbius transformation
Growth control
Gradient

ABSTRACT

I show that Arabidopsis leaf growth can be described with good precision by a conformal map, where expansion is locally isotropic (the same in all directions) but the amount of expansion can vary with position. Data obtained by tracking leaf growth over time can be reproduced with almost 90% accuracy by such a map. The growth follows a Möbius transformation, which is a type of conformal map that would arise if there were an underlying linear gradient of growth rate. From the data one can derive the parameters that describe this linear gradient and show how it changes over time. Such a rule has the property of maintaining the flatness of a leaf.

1. Introduction

The study of leaf growth has a long history (Goebel, 1905), and mapping the process has become increasingly precise over the years (Avery, 1933; Richards and Kavanagh, 1943; Erickson, 1966; Rolland-Lagan et al., 2003; Remmler and Rolland-Lagan, 2012; Rolland-Lagan et al., 2014; Cui et al., 2010; Green et al., 2010; Kennaway et al., 2011; Kuchen et al., 2012; Sauret-Gueto et al., 2013). The pattern of leaf growth has been accounted for by models in which growth regulators operate within specified regions of the leaf (Kuchen et al., 2012), polarity fields control the predominant direction of growth (Sauret-Gueto et al., 2013), and gene networks regulate the succession of morphogenetic events in a combinatorial fashion (Cui et al., 2010; Green et al., 2010; Sauret-Gueto et al., 2013).

A different type of explanation, with its roots in physics and engineering, goes back to D'Arcy Thompson and his famous book, On Growth and Form (Thompson, 1917). Thompson discusses leaf growth in terms of transformations extending over the whole leaf area, and points to possible underlying physical mechanisms. In a footnote (Thompson, 1917, p. 1084), he draws attention to the resemblance of certain mappings to conformal transformations. These are transformations of the plane that preserve angles locally, and are generated by isotropic local expansion. The amount of expansion can vary with position, but at any point expansion occurs to the same extent in all directions. Conformal maps are very important in physics and engineering, because they are intimately connected with diffusion, hydrodynamics and electrical fields. There is also a close connection with complex analytic functions, which are maps from the complex plane to itself (the complex plane, or Argand diagram, represents complex numbers $x + iy$). Every complex analytic function is conformal and vice-versa.

By comparison, conformal maps have played only a small part in the study of biological structures. There is an intriguing paper

E-mail address: gjm12@cam.ac.uk

http://dx.doi.org/10.1016/j.jtbi.2016.08.023

by Schwartz (1977), showing that the mapping of retinal ganglion cells to the cortex or the optic tectum can be well approximated by a complex logarithm. And more recently, Jones and Mahadevan (2013) revived and generalised D'Arcy Thompson's approach by considering the larger class of quasi-conformal mappings, where the expansion is not necessarily isotropic. They show how to use these mappings for various kinds of morphometry.

Another contribution comes from Wolfram, in a footnote in his magnum opus A New Kind of Science (Wolfram, 2002), where he proposes that leaf growth might follow a conformal mapping, pointing out that this would preserve the flatness of the leaf surface. He also observes that conformal mappings might be generated biologically by a diffusion-based mechanism, arguing that the growth rate underlying such a mapping must satisfy the equilibrium diffusion equation.

In a certain sense, Wolfram's assertion about flatness is a tautology, since a conformal map is planar and a planar map will preserve flatness. The real content lies in the proposal that leaf growth is locally isotropic. If this is true, then to be planar amounts to being conformal. Erickson (1966), using Avery's classic data on the growth of tobacco leaves (Avery, 1933), concluded that leaf growth was largely isotropic, but the leaves in question were large (several centimetres in length), and Richards and Kavanagh (1943) emphasise that early leaf growth is 'strongly non-isotropic' in contrast to the later stages. This is supported by more recent work using clones, which become markedly elongated in petals (Fig. 2 in Sauret-Gueto et al., 2013) and leaves (Fig. 2 in Kuchen et al., 2012). At first sight, therefore, it seems unlikely that early leaf growth can be treated as locally isotropic.

The surprise is that Wolfram's assumption turns out to be largely correct. I show here that, using data kindly made available by Professor Rolland-Lagan, that the growth of *Arabidopsis* leaves approximates remarkably well to a conformal mapping, about 90% of the growth being accounted for by such a map. A fascinating question is then raised by the relationship between this kind of explanation and the gene-based interpretation discussed initially.

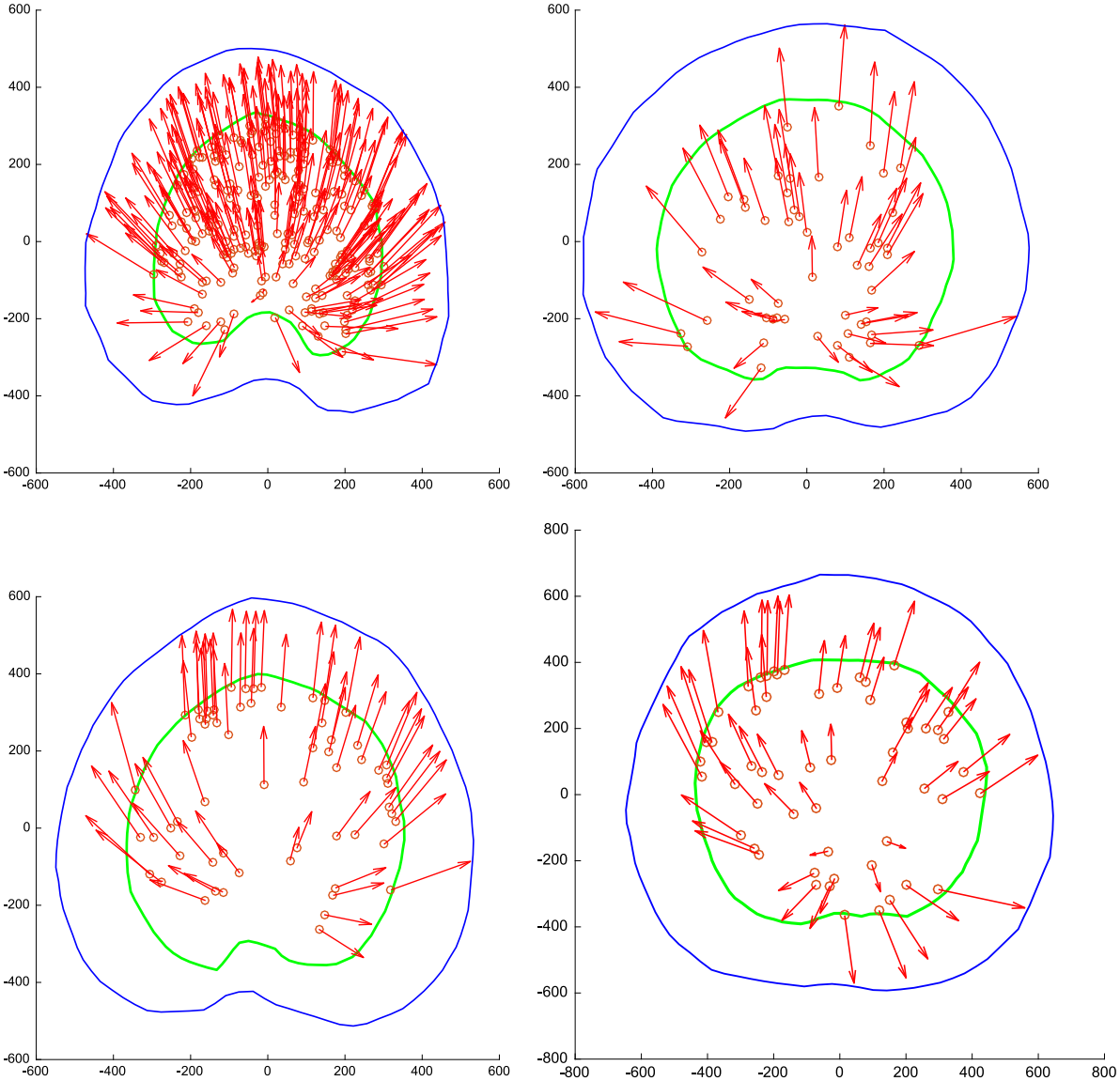

Fig. 1. The displacement of beads between day 7 and day 8 for four leaves, the one with the greatest number of beads (leaf 1) and three others. The green outline is the margin of the leaf at day 7 and the blue outline that at day 8. The beads are shown as small circles at the start of the arrow, which ends at the position of that bead at day 8. The axes show the size of the leaves in microns. Note that the origin of the *x*- and *y*-coordinates lies at the approximate centre of the leaves.

2. The pattern of local growth

The data used here consist of a set of observations of individual *Arabidopsis* leaves (Remmler and Rolland-Lagan, 2012; Rolland-Lagan et al., 2014), each of which has a number of beads attached to its surface that are tracked day by day (see Appendix A.1). The earliest time point is day 7 after sowing, and there are altogether thirteen leaves that were tracked till day 12. As we shall see, the earliest time step, day 7 to day 8, provides the most interesting data, since uniform expansion, with a constant relative growth rate (RGR) over the entire leaf, increasingly takes over with increasing age. Fig. 1 shows the displacement of beads between days 7 and 8 for several leaves.

We would like to understand these maps at the level of individual cells and their growth rates. To do this, we need to characterise the local growth map, i.e. the way that tissues expand on a small scale. This information is captured by the derivatives of the map and in particular by the Jacobian matrix, which is the analogue, for growth between two time points, of the growth tensor (Kennaway et al., 2011). If we write the map as $(x, y) \rightarrow (u(x, y), v(x, y))$, then the Jacobian J is defined by

$$J = \begin{pmatrix} u_x & u_y \\ v_x & v_y \end{pmatrix} \tag{1}$$

where u_x stands for $\partial u/\partial x$, u_y for $\partial u/\partial y$, and so on.

We are particularly interested in those growth rules that lead to a flat leaf surface, since many leaves are approximately flat, including the *Arabidopsis* leaves in our data set (e.g. see Fig. 3 of Rolland-Lagan et al., 2014). Some of the growth rules of this type lead to a distinctive form for the Jacobian. For example, suppose that the rate of growth is the same at every point of the leaf lamina. The growth could be anisotropic (greater along one axis than the other), but the amount of growth is assumed not to vary with position. Fig. 2A shows an example of such growth applied to an initial square array; each small square expands to a larger rectangle and these all have identical shape. If growth is by a factor a along the x-axis and by a factor b along the y-axis, the Jacobian at every point is:

$$J = \begin{pmatrix} a & 0 \\ 0 & b \end{pmatrix} \tag{2}$$

Another type of map has properties that are in a sense the opposite of the foregoing: the growth rate does not have to be constant over the leaf surface, but it is locally isotropic. Fig. 2B shows an example; notice how each small square deforms into a square (approximately) because of local isotropy. Notice also that the greater growth at the bottom of the grid leads to rotation of the small squares. This is passive rotation produced by expansion of adjacent tissue (Kennaway et al., 2011). The matrix for rotation through an angle θ is $A = \begin{pmatrix} \cos\theta, & -\sin\theta \\ \sin\theta, & \cos\theta \end{pmatrix}$. When combined with the effect of isotropic relative growth $g(x, y)$, this gives rise to a Jacobian of the form

$$J = \begin{pmatrix} a(x, y) & -b(x, y) \\ b(x, y) & a(x, y) \end{pmatrix} \tag{3}$$

where $a(x, y) = g(x, y)\cos\theta(x, y)$ and $b(x, y) = g(x, y)\sin\theta(x, y)$. Comparing Eq. (3) with Eq. (1) shows that $u_x = v_y$ and $u_y = -v_x$. These are the celebrated Cauchy-Riemann equations that define a conformal map; Appendix A.2.

The next question is whether the Jacobian calculated for the observed leaf growth has a distinctive signature. Fig. 3 shows that there is a striking agreement with the conformal pattern (see Appendix A.3). The top left (u_x) and bottom right (v_y) derivatives are roughly equal, as expected from Eq. (3), and are positive (red) because $a = g\cos\theta$ and both g and $\cos\theta$ are positive. Whereas the top right (u_y) and bottom left (v_x) derivatives are of opposite sign (blue is negative), also as expected from Eq. (3). The fact that the signs switch around the midvein is a consequence of the symmetry of the leaf shape and the fact that growth leads to rotations in opposite directions in the two halves of the leaf. The other leaves show similar patterns, though with considerably more noise in the relationship between u_y and v_x; see the last two columns in Table A2. This may partly be explained by the smaller size, and hence vulnerability to noise, of these components compared to u_x and v_y (note the difference in scale in Fig. 3).

It is interesting to compare these patterns to earlier observations of growth rates and vorticity (Richards and Kavanagh, 1943; Erickson, 1966; Silk and Erickson, 1979) (see Appendix A.5 for explanations of these quantities). These authors plotted the divergence $(u_x + v_y)$ and the vorticity $\frac{1}{2}(v_x - u_y)$ in various leaves, and found patterns resembling those in Fig. 3, namely larger values of the divergence towards the base of the leaf and opposite patterns of vorticity around the midline (see Silk and Erickson, 1979, Fig. 3). They were not, however, measuring what for us are the crucial variables, namely the individual components in the divergence and vorticity. The divergence will not reveal whether u_x and v_y are equal; it just gives their sum. Likewise, the vorticity will not reveal whether $u_y = -v_x$, but if this Cauchy-Riemann equation does hold then the vorticity will coincide with v_x (or $-u_y$).

3. Fitting a conformal map to growth

In the preceding section we found that the growth map has the characteristics of a conformal map. Our strategy now will be to find the conformal map that best fits the data.

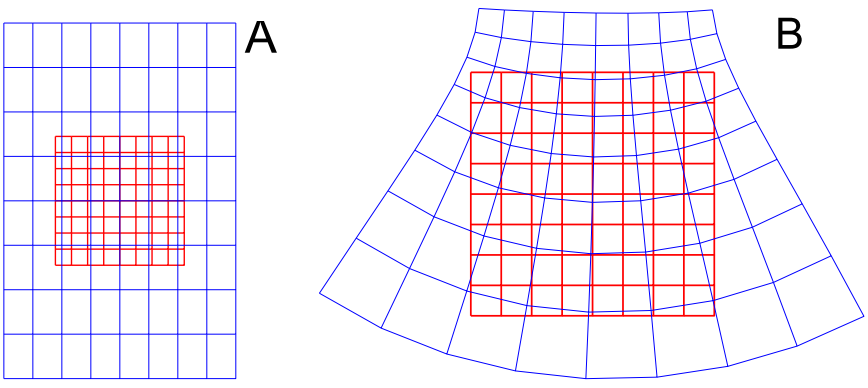

Fig. 2. Some examples of growth maps that preserve the flatness of a leaf. A: growth is the same at all points, but can be anisotropic. B: growth is isotropic, but the growth rate can vary with position. In this case, the growth rate increases as one moves downwards, and this causes the tissue to rotate.

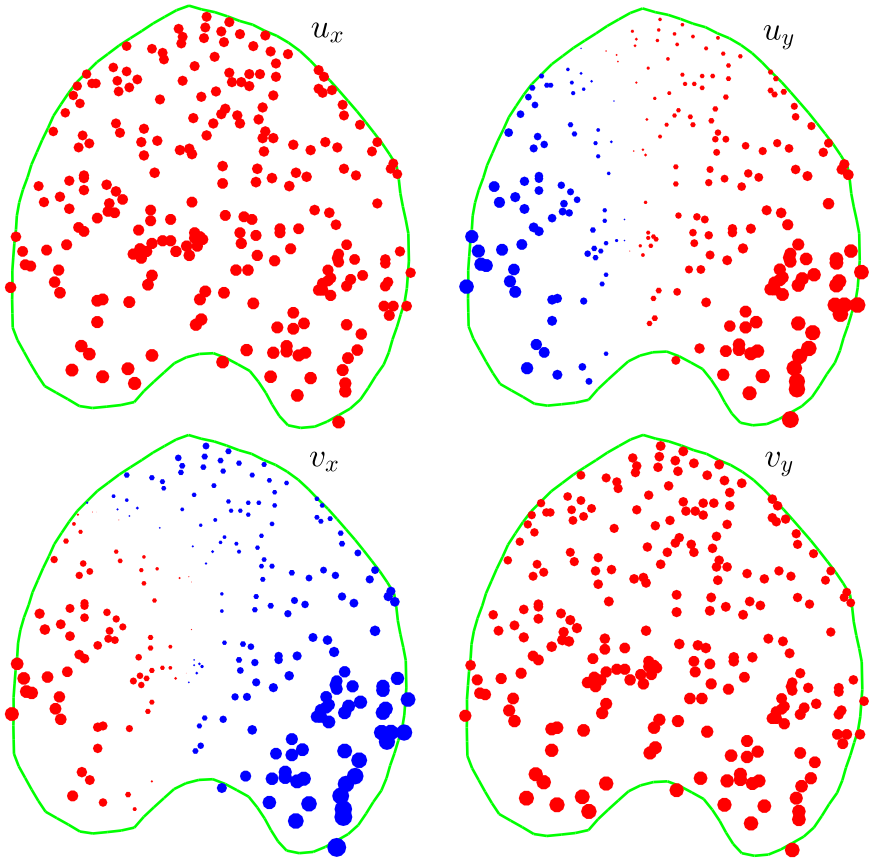

Fig. 3. The components of the Jacobian, Eq. (3), the linear transformation that defines the local expansion and rotation due to growth. This is based on the data for leaf 1 shown in Fig. 1. The radius of the beads is the (scaled) size of the derivative, with red for positive values and blue for negative. The 'a' components (u_x and v_y) have been displayed at 1/4 the scale of the 'b' components (u_y and v_x).

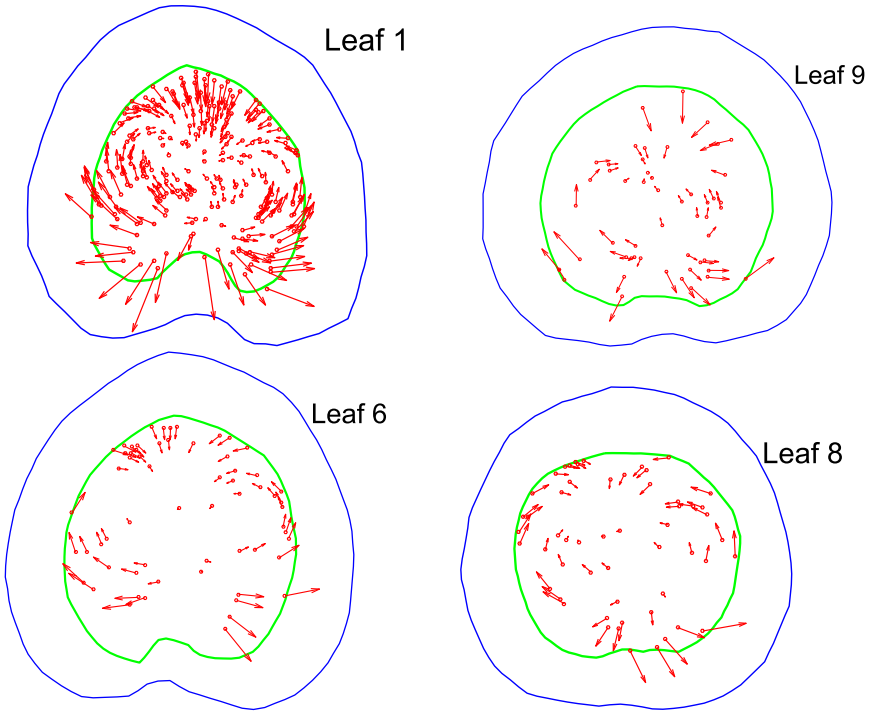

Fig. 4. The residual movement of beads after subtracting the best-fitting linear map, for four leaves and the time period 7–8 days. Note the rotation of the arrows at twice the speed of the radius, and compare with the quadratic function in Fig. 5.

We have seen that the Jacobian signature of conformal growth is equivalent to the Cauchy-Riemann equations. These tell us that a conformal map can be regarded as a complex analytic function (see Appendix A.2 and Eqs. (A1) and (A2)). Given this, our strategy will be to interpret the plane in which a leaf grows as the complex plane. This means that a point with coordinates (x,y) is regarded as the complex number $z = x + iy$ (Needham, 1997). We can then look at any function of z, e.g. a polynomial $a + bz + cz^2$, as a map from the complex plane to itself, and we can ask how well this approximates the growth of the leaf – regarding this also as a map of the complex plane to itself. By varying the coefficients a, b and c (which are themselves complex numbers) we can find the polynomial that minimises the error in predicting the positions of the beads.

Consider the linear function $f(z) = a + bz$, where $z = x + iy$, and $a = a_0 + ia_1$ and $b = b_0 + ib_1$ are complex constants. This map takes the point (x,y) to (u,v), where $u = a_0 + b_0x - b_1y$ and $v = a_1 + b_0y + b_1x$. This amounts to a shift of origin to the point a in the complex plane, a rotation by $\arg b = \arctan(b_1/b_0)$, and a constant RGR everywhere on the leaf of $|b| = \sqrt{b_0^2 + b_1^2}$. Thus a linear complex map can capture the relative positioning and orientation of the leaf between successive days, which have to do with the experimental set-up; it can also account for a constant RGR, which is a parameter with biological significance.

Thus the best-fitting linear complex map, found by least squares fitting of the bead data points (see Appendix A.4), gives us an estimate of both the experimental parameters and the intrinsic uniform isotropic growth. The difference between the final bead position predicted by this linear model and the true position, i.e. the linear model *residual*, indicates how much of the growth involves variation of growth rate with position in the leaf, with consequent rotation of the tissue, as depicted in Fig. 2B. The size of this residual can be measured by summing the lengths of the residual vectors and dividing this by the sum of the total bead displacement observed experimentally. This *normalised residual* has an average value over all the leaves of 0.33; see Table A2. Equivalently, one can say that 67% of the displacement is accounted for by a linear model.

The distribution of this residual over the leaf lamina is shown in Fig. 4. This is very striking: as one follows a path round the perimeter of the leaf, the residual vectors rotate *twice as fast* as the radial vector. This is what is expected of a quadratic complex function, as shown in Fig. 5. Note that the origin of the leaf's coordinate system is in the approximate centre of the leaf, and that of the complex quadratic lies at the centre of the circle.

Given this pattern in the residual, we expect to get a better fit to the data with a quadratic complex polynomial $f(z) = a + bz + cz^2$, and this is indeed the case, as shown by the substantially smaller normalised quadratic residuals in Table A2, with an average of 0.14, (86% of the displacement accounted for). Adding a cubic term, $f(z) = a + bz + cz^2 + dz^3$, gives a further small improvement, with 0.11 residual or 89% of the displacement accounted for; see Table A2. Additional higher power terms give negligible improvement.

In addition to fitting a polynomial, one can also fit a Möbius transformation (Needham, 1997; Arnold and Rogness, 2008), which has the form

$$f(z) = \frac{a + bz}{c + dz}, \tag{4}$$

where a, b, c and d are complex numbers. Möbius transformations have the attractive property that the composition of two of them – i.e. following one by the other – is again a Möbius transformation. Furthermore, they have a matrix representation that is very useful for interpolating between the observations, as will be discussed later. It turns out that one gets almost as good a fit from a Möbius transformation as from a cubic, with an average residual of 0.12, or 88% of displacement accounted for; see Table A2.

To summarise so far, a linear conformal map, which is equivalent to constant RGR, can account for about 67% of the displacement of beads, whereas a nonlinear conformal map, cubic or Möbius, accounts for 88–89% of the displacement (these are figures averaged over all leaves, for days 7–8). There is therefore a substantial nonlinear component to the conformal growth.

The fact that the observed growth is mostly conformal is a strong statement about the growth of the leaves: the basic mechanism of leaf growth must be able to generate such a map. It also tells us something about the residual, i.e the remaining small part of the map that is not conformal. In many of the leaves this highlights regions where some kind of systematic directional growth is concentrated. As can be seen from Fig. 6, there is considerable variation between individual leaves, some having marked anisotropic basal growth and others having very little. Basally localised anisotropic growth has previously been observed in averaged leaf data, e.g. Fig. 7 in Remmler and Rolland-Lagan (2012). What is new here is the large amount of individual variability in this anisotropic component.

The leaves also show a strong basal bias in the *isotropic* growth rate, which can be seen in the best-fitting conformal map. Unlike anisotropic growth, this pattern is found in all the leaves. This is well documented in the literature (Kuchen et al., 2012; Rolland-Lagan et al., 2014), though fitting a conformal map clarifies the distinction between oriented and isotropic components in this gradient.

The data set allows one to follow the pattern of residuals for five successive time steps, beginning with 7–8 days. Fig. 7 shows residuals averaged over all leaves: the linear residual gets steadily

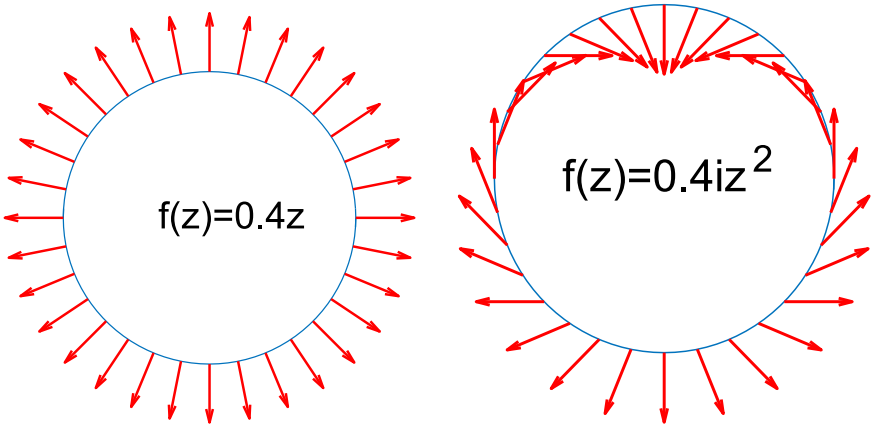

Fig. 5. Two complex functions, represented by arrows: the linear function, $f(z) = 0.4z$ and the quadratic one $f(z) = 0.4iz^2$.

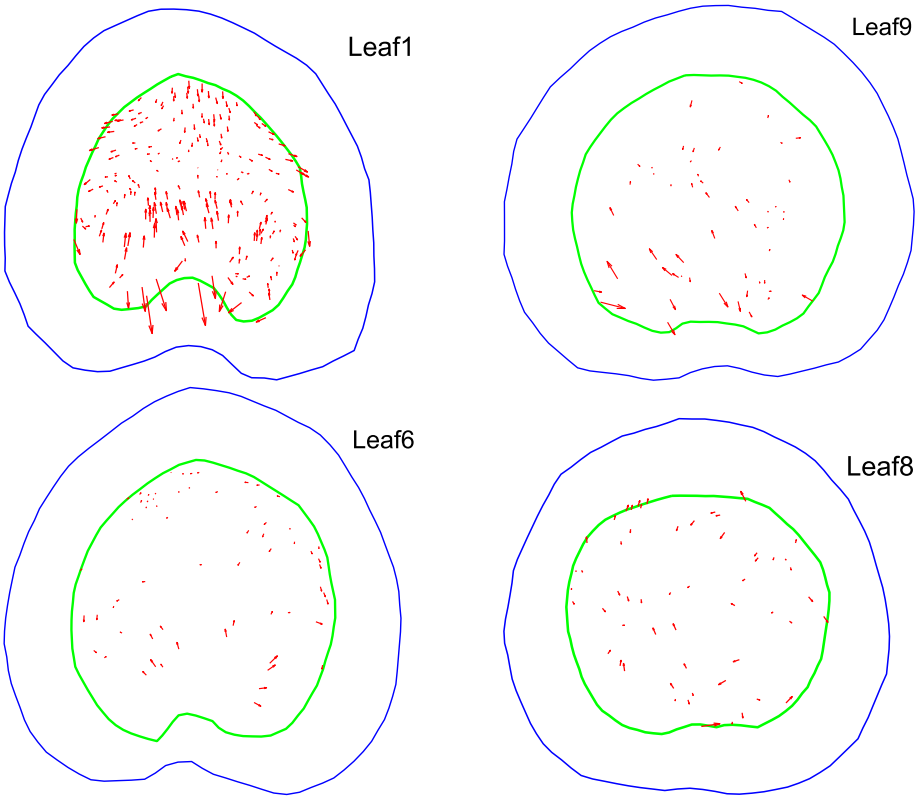

Fig. 6. The residual from the best fitting complex polynomial, for four leaves from days 7–8. The small circles representing beads have been removed so that the arrows can be seen more clearly.

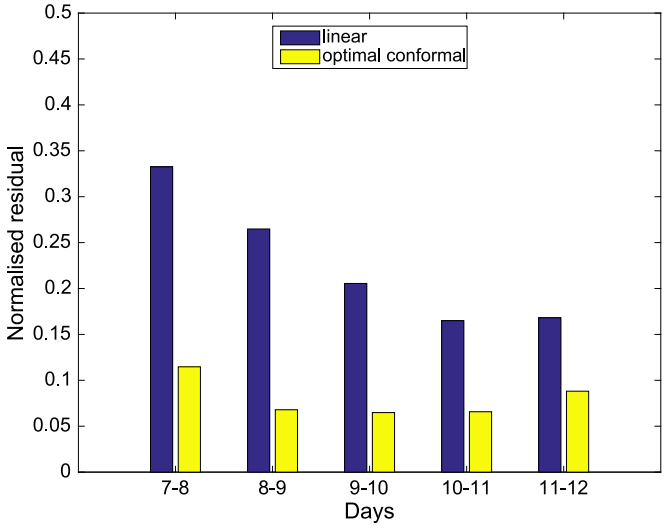

Fig. 7. Change in the average residuals (linear and cubic) over time, showing the decrease in the linear residuals, and hence the increasingly large component of constant RGR, as the leaves age.

smaller, implying that the component of constant RGR increases steadily, so that some 85% of the growth is constant expansion by days 11–12. The pattern of linear residuals for an individual leaf (leaf 1) over five successive days is shown in Fig. 8, and it tells the same story, with the initially large residuals at the apex and base of the leaf gradually diminishing.

4. The biological meaning of conformal growth

A conformal map is a very special type of map, and it is natural to ask how it could be generated biologically. Wolfram's answer (Wolfram, 2002) is that conformal growth will occur precisely when the RGR has the special property of being a harmonic function, i.e. when it satisfies the equilibrium equation for diffusion (see Appendices A.6 and A.7). He also proposed that the RGR might therefore be specified by the concentration of a diffusing signal molecule, though I will point out some difficulties with this proposal in due course.

Now it turns out that for the leaves in our data set the conformal component of their growth is well approximated by a Möbius function, Eq. (4), and that the underlying RGR that generates these functions is of a particularly simple kind, namely a linear gradient (see Appendix A.8). All that is required, therefore, is that cells set their RGR – their rate of isotropic expansive growth – according to a linear gradient at any moment in time. A linear gradient is a harmonic function, but a very special one.

Let us run through the steps that lead to this conclusion. A Möbius function (Needham, 1997; Arnold and Rogness, 2008) has the attractive property that one can 'wind back the clock' and recreate intermediate steps in the growth pattern. This is possible because one can associate to the Möbius transformation $f(z) = (a + bz)/(c + dz)$ the matrix $F = \left(\begin{smallmatrix} b & a \\ d & c \end{smallmatrix}\right)$, and composing two Möbius transformations is equivalent to multiplying their matrices. Thus given an observed map over some time period (24 h for the data used here), one can take a fractional power of the associated matrix and estimate the map for a shorter time period than the original 24 h (for background on fractional powers of matrices and Möbius transformations, see Appendix A.9). Fig. 9 illustrates the method by taking the square root of the matrix A for the best-fitting Möbius transformation for leaf 4 between days 7 and 8; the matrix $\sqrt{A}$ gives an estimate of growth in half the period of observation, i.e. 12 h.

By taking smaller fractional powers one retrieves the growth pattern for shorter times, and in the limit this enables one to

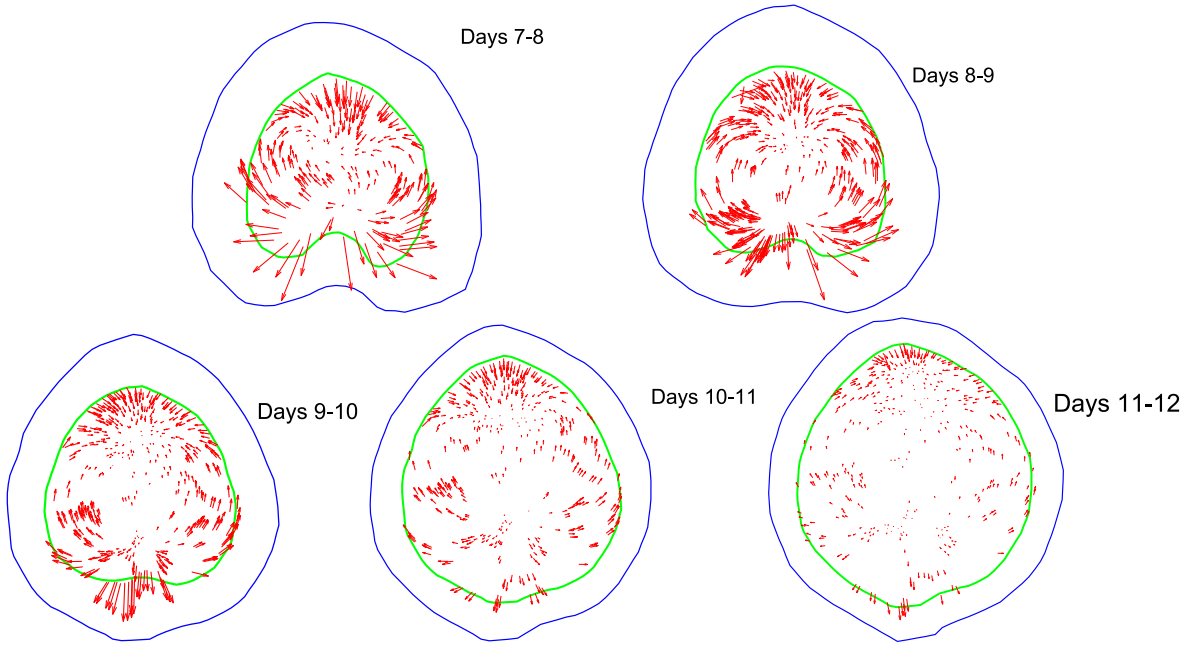

Fig. 8. The linear residual for leaf 1 from day 7 to day 12.

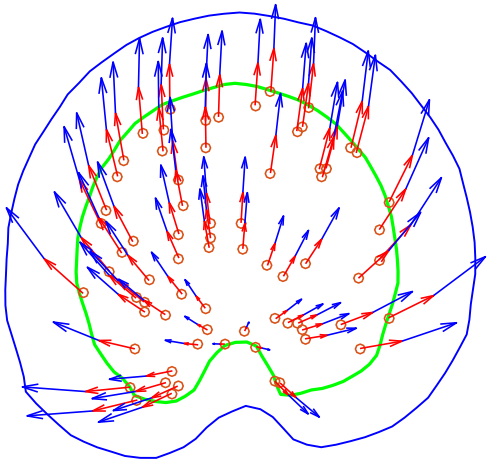

Fig. 9. Factorising the growth into two 12 h periods, using the Möbius transformation with matrix $\sqrt{A}$, where A represents the best fit for the 24 h between days 7 and 8 (leaf 4). The composition of the two maps, i.e. the result of following the red arrows and then the blue arrows, is equivalent to the 24 h best fit.

Table 1
The constants specifying the linear gradient in the RGR for leaf 1 over five successive day-lengths. The gradient is given by Eq. (A.16) as $RGR(x, y) = (b_0 - c_0) - 2d_0x - 2d_1y$. Growth is over 24 h, so the units for $b_0 - c_0$ are per day, and for d_0 and d_1 are per millimetre per day.

days			$b_0 - c_0$
d_0	d_1		
7–8	0.4457	0.038	0.574
8–9	0.4362	0.015	0.271
9–10	0.3391	0.004	0.120
10–11	0.2686	-0.006	0.051
11–12	0.2099	0.003	0.026

calculate the infinitesimal generator (Eqs. (A9), (A12) and (A15)), and hence the distribution of the RGR everywhere on the leaf. A straightforward calculation, Eq. (A.16), shows that the RGR distribution is linear, that is to say, linear in cartesian (rectangular) coordinates, not, for example, in polar coordinates. It is possible to estimate the constants that determine this linear gradient from the bead movements. Table 1 gives these constants for leaf 1 over five successive day periods. There is a steady decrease in the average growth rate with time, $(b_0 - c_0)$, and also a decrease in the slope in the direction of the leaf axis, d_1, which accords with the decreasing nonlinear terms shown in Figs. 7 and 8. Fig. 10A and B show what the gradients look like for this particular leaf.

5. Discussion

The growth patterns of the leaves studied here have a significant nonlinear component (Fig. 4), yet it turns out that they can be explained by a linear gradient of growth rate (Fig. 10A and B), that is to say, a gradient that is linear in cartesian coordinates and not, for instance, in polar coordinates (which would not generate a conformal map). It is interesting to ask how this linear gradient could be generated. Linear gradients of a diffusible signal molecule were originally postulated as the underlying mechanism for pattern formation (Lawrence, 1966; Wolpert, 1969), and this seems natural for certain geometries, e.g. a segment in an insect embryo, since diffusion will interpolate in a linear fashion between a source and sink. However, a linear diffusion gradient in a leaf can only arise in a somewhat contrived way, since the outline of the leaf is irregular, and there needs to be a special layout of sources and sinks to ensure linearity (see Fig. 11). Furthermore, the gradients that have been found are not linear; in the case of Bicoid, the gradient is exponential (Driever and Nüsslein-Volhard, 1988, 1988; Gregor et al., 2007).

Thus Wolfram's (2002) proposal of read-out of the RGR from an equilibrium diffusion gradient seems implausible here, though one abandons this idea with regret since it would have meant that any source or sink arrangement on the margin of a leaf would create a signal distribution that was guaranteed to produce a conformal map and hence a flat leaf. If this is not the explanation, then it is an intriguing question what mechanism leads to a linear gradient of RGR over the leaf lamina. It also invites investigation of other leaves to see if their growth is also conformal and whether it is also well approximated by a Möbius transformation.

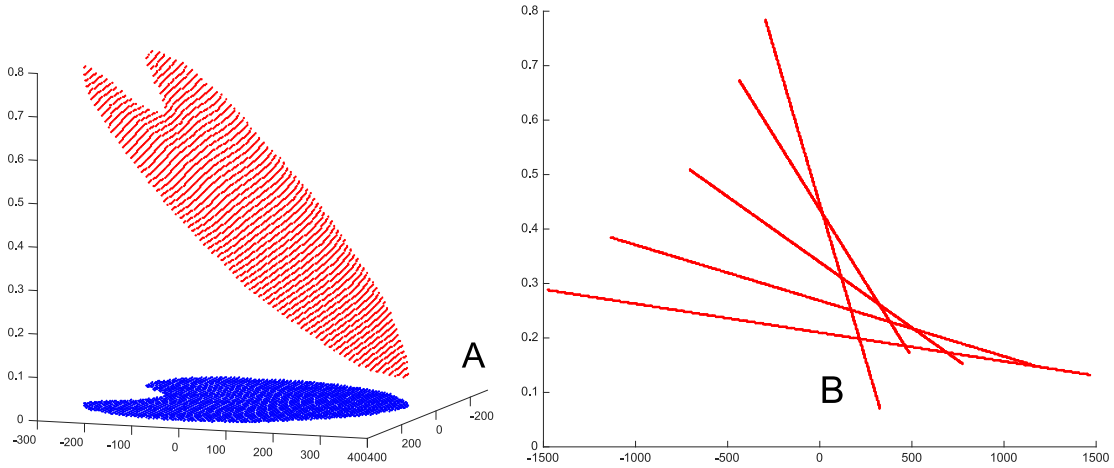

Fig. 10. A: The linear gradient in RGR. Its minimum value is at the distal tip of the leaf, where growth is slowest, and its largest values at the base. B: The gradual flattening of the gradient in RGR with successive days. Each line represents the gradient along the midvein.

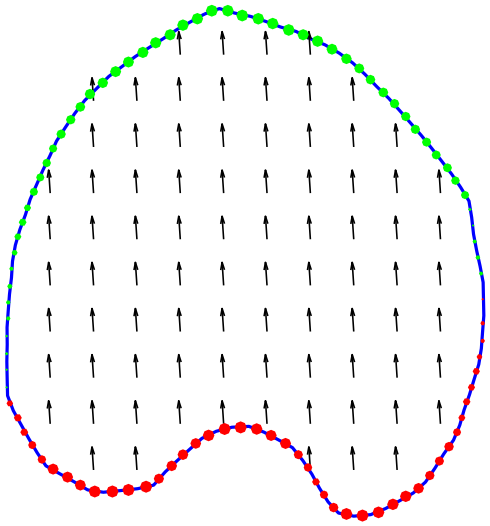

Fig. 11. The flux pattern associated to a linear gradient set up by diffusion, and the distribution of sources (red) and sinks (green), calculated for the outline of leaf 1, that would be needed to generate the gradient. (For interpretation of the references to colour in this figure legend, the reader is referred to the web version of this article.)

There is already a fairly detailed analysis of leaf growth in terms of developmental programs (Rolland-Lagan et al., 2003; Remmler and Rolland-Lagan, 2012; Rolland-Lagan et al., 2014; Cui et al., 2010; Green et al., 2010; Kennaway et al., 2011; Kuchen et al., 2012; Sauret-Gueto et al., 2013), and it would be interesting to bring this into register with the fact that growth is largely conformal. One obvious question is how the local isotropy of a conformal map can be reconciled with the elongation of clones in Kuchen et al. (2012). A different staging criterion is used in Kuchen et al. (2012) and Remmler and Rolland-Lagan (2012); Rolland-Lagan et al. (2014). However, judging by leaf size, 6 DAI ('days after initiation') in Kuchen et al. (2012) corresponds to day 7 in our data set from Remmler and Rolland-Lagan (2012), Rolland-Lagan et al. (2014), where 'days after sowing' are used. The elongated clones seen on 6 DAI (Fig. 2A, Kuchen et al., 2012) were initiated 3 days earlier, so a 2:1 elongation factor over 3 days, which seems a reasonable estimate by eye, would require an elongation factor of $\sqrt[3]{2} \approx 1.26$ per 24 h. Thus, if λ and μ denote the relative growth in 24 h along the axis of the leaf and in the orthogonal direction, respectively, we require $\lambda/\mu = 1.26$. Now consider a simplified model in which these growth rates are constant over the leaf, and where the conformal model has a constant relative growth per 24 h of $(\lambda + \mu)/2$. Then if we represent the collection of beads by two instances, one bead on the y-axis and another of the x-axis, the normalised residual (Table A2) is $(\lambda - \mu)/(\lambda + \mu)$. Equating this to the average value of the cubic residual, 0.12, we get $\lambda/\mu = 1.27$, which is not far from the value given above for achieving a 2:1 anisotropy in the clones. Thus there need be no contradiction between the elongation of clones over 3 days of growth and the good match achieved by a conformal map.

Turning to the network of factors controlling growth hypothesised in Kuchen et al. (2012), can the action of the factors PGRAD and LATE be explained by the linear growth rate in the conformal picture and its diminishing slope with time (Table 1 and Fig. 10)? One difference is that PGRAD levels are assumed to be inherited by lineage and therefore to deform with the growth of the tissue (Kuchen et al., 2012), whereas the linear RGR in our conformal picture changes dynamically with time so as to maintain its linearity. There is also no indication of a distinction between lamina and midvein growth (formalised by the factors LAM and MID Kuchen et al., 2012) in the residuals from the best-fitting conformal map (e.g. Fig. 6). However, this may just be a matter of resolution, since the domain of operation of MID is quite narrow.

It would be interesting to understand how the mechanism proposed to explain indentations in *Arabidopsis* leaves (Bilsborough et al., 2011; Engelhorn et al., 2012) fits with a conformal viewpoint. Is this a developmental subroutine added onto the conformal growth plan of the lamina, or is it integrated into the underlying RGR distribution to make a complete conformal map?

Finally, one would like to extend these ideas to the realm of curved surfaces, since a flat leaf is only a special case of a large variety of three-dimensional leaf or petal shapes seen in the plant world. Some steps have been taken in this direction: a framework for combining genetic growth rules and physical constraints has been proposed (Green et al., 2010; Kennaway et al., 2011), and the mechanics of leaves has been modelled using the theory of thin elastic plates (Mahadevan and Liang, 2009; Liang and Mahadevan, 2011). How can the notion of a conformal map be extended to the realm of curved surfaces? Wolfram's approach gives a useful clue, by relating the curvature to the growth rate (see Appendix A.7), thus suggesting possible mechanisms for making curved surfaces.

Acknowledgements

I thank Anne-Gaëlle Rolland-Lagan for allowing me to use her data, Benoit Tremblay for help with the Matlab package that

allows one to manipulate the data, Konrad Wagstyl for an introduction to Matlab programming, and Julie Ahringer, Dennis Bray, Richard Durbin, Jeremy Gunawardena and Ottoline Leyser for helpful comments on the manuscript. I also thank one of the reviewers for suggesting the calculation in the Discussion that reconciles the anisotropy of clones with the conformal model.

A.1. Data and data-analysis programs

The two papers from Prof. Rolland-Lagan's laboratory, (Remmler and Rolland-Lagan, 2012; Rolland-Lagan et al., 2014), give a thorough description of growth patterns and point the reader towards a website (http://hdl.handle.net/10393/30401) where the bead data for individual leaves are available, and also a package of Matlab programs for leaf shape analysis. Leaves are referred to by pot and plant numbers in their data sets, and Table A1 shows how this relates to the numbering used here.

Table A1
The numbering of leaves used here (in order of decreasing number of beads), and the numbering in Remmler and Rolland-Lagan (2012), Rolland-Lagan et al. (2014), defined by the pot and plant. Also given is the number of beads on each leaf.

My numbering	POT	PLANT	Number of beads
1	19	1	231
2	19	2	82
3	1	2	80
4	3	3	71
5	7	1	68
6	3	2	62
7	3	1	57
8	7	2	55
9	5	1	51
10	20	1	36
11	17	1	32
12	1	1	26
13	7	3	22

A.2. Complex functions and their derivatives

Let f be a complex analytic function. This means that f is differentiable as a complex function (as are all the functions one is likely to encounter in the present context). We can write the function in terms of its real and imaginary parts as $f(x, y) = u(x, y) + iv(x, y)$, where $x + iy$ is the point with coordinates x, y in the complex plane. Calculating the derivative of f by a real δx gives $f' = u_x + iv_x$ (where u_x denotes $\partial u/\partial x$, etc.), whereas making the calculating with an imaginary $i\delta y$ gives $f' = -iu_y + v_y$. Equating these two definitions yields the Cauchy-Riemann equations,

$$u_x = v_y, \tag{A.1}$$

$$u_y = -v_x. \tag{A.2}$$

These in turn imply that

$$u_{xx} + u_{yy} = 0, \tag{A.3}$$

$$v_{xx} + v_{yy} = 0, \tag{A.4}$$

(where $u_{xx} = \partial^2 u/\partial x^2$, etc.), showing that both u and v satisfy Laplace's equation, which is the equation for the equilibrium distribution of a diffusing substance (Crank, 1975). A function satisfying this equation is called a *harmonic* function. Thus both the real and imaginary parts of f are harmonic. Conversely, given a harmonic function u, the Cauchy-Riemann equations can always be solved to give v, and this yields a conformal map with real and imaginary parts u and v.

Table A2
Normalised residuals after least-squares fitting to linear, quadratic or cubic complex polynomials and a Möbius transformation. The normalised residual is defined as $\sum_k |v_k - l_k| / \sum_k |v_k|$, where v_k is the vector between bead positions on successive days, l_k is the vector predicted by the complex function, and k runs over all beads. Also shown are the measures $E(u_x, v_y)$ and $E(u_y, v_x)$ of accuracy with which the Cauchy-Riemann equations $u_x = v_y$ and $u_y = -v_x$ hold; see Eqs. (A.6) and (A.7). If $E = 0$, the relevant equation holds exactly for every bead. As can be seen, $E(u_x, v_y)$ is small, whereas $E(u_y, v_x)$ is larger, especially for leaves 5, 11 and 12. Leaves 5 and 11 also have large cubic and Möbius residuals.

Leaf	Linear residual	Quadratic residual	Cubic residual	Möbius residual		$E(u_y, v_x)$
		$E(u_x, v_y)$				
1	0.289	0.124	0.101	0.103	0.090	0.058
2	0.449	0.202	0.141	0.148	0.307	0.072
3	0.381	0.158	0.135	0.130	0.434	0.112
4	0.376	0.164	0.138	0.141	0.342	0.072
5	0.406	0.209	0.165	0.178	0.546	0.094
6	0.247	0.083	0.052	0.065	0.154	0.044
7	0.325	0.117	0.110	0.112	0.221	0.043
8	0.348	0.145	0.092	0.116	0.231	0.047
9	0.301	0.121	0.099	0.107	0.309	0.070
10	0.261	0.123	0.097	0.118	0.226	0.061
11	0.360	0.178	0.180	0.193	0.608	0.092
12	0.253	0.101	0.101	0.105	0.716	0.081
13	0.327	0.104	0.080	0.088	0.272	0.018
Average	0.333	0.141	0.115	0.123	0.343	0.067

A.3. Calculating derivatives

To compute the terms in the Jacobian, Eq. (1), at each bead we need to estimate the derivatives u_x, u_y, v_x, and v_y. For this we need a map $(x, y) \to (u(x, y), v(x, y))$ that interpolates smoothly between the values at beads. Following Rolland-Lagan et al. (2014), we assume that u and v are each third-order polynomials in x and y, and choose values of the polynomial coefficients that minimise the sum-of-squares error. If the coordinates of bead k at time 1 are $(x_1^{(k)}, y_1^{(k)})$ and at time 2 are $(x_2^{(k)}, y_2^{(k)})$, the error is given by:

$$S = \sum_k \left(u(x_1^{(k)}, y_1^{(k)}) - x_2^{(k)} \right)^2 + \left(v(x_1^{(k)}, y_1^{(k)}) - y_2^{(k)} \right)^2, \tag{A.5}$$

where the index k runs over all beads. The minimisation is a linear problem that can be done very rapidly by linear algebra functions in Matlab.

No assumption is made about the form of the polynomials, and there is no presumption that they lead to a conformal map. However, as Fig. 3 shows, for leaf 1 the map shows the diagnostic sign pattern of A conformal map. To quantify this for all the leaves, we would like to test how precisely the Cauchy-Riemann equations $u_x = v_y$, $u_y = -v_x$ hold. One way to quantify this is to take the absolute value of the differences $|u_x - v_y|$ and $|u_y + v_x|$, evaluated at each bead position, and suitably normalised. More precisely we take

$$E(u_x, v_y) = \left(\sum_k |u_x^k - v_y^k| \right) / \left(\sum_k |u_x^k| + |v_y^k| \right), \tag{A.6}$$

$$E(u_y, v_x) = \left(\sum_k |u_y^k + v_x^k| \right) / \left(\sum_k |u_y^k| + |v_x^k| \right), \tag{A.7}$$

where k runs over all beads. Then $E(u_x, v_y)$ and $E(u_y, v_x)$ lie between 0 and 1, and $E(u_x, v_y) = 0$ means that $u_x = v_y$ holds precisely for all beads, and similarly $E(u_y, v_x) = 0$ means that $u_y = -v_x$ for all the beads. The last column of Table A2 shows that $E(u_x, v_y)$ is close to zero for all leaves. The last column but one of Table A2 shows that $E(u_y, v_x)$ is generally larger, which can be partly accounted for by the fact that the derivatives u_y and v_x are on average about 4 times smaller in absolute magnitude than u_x and v_y, (different scales have been used in Fig. 3). $E(u_y, v_x)$ for leaves 5, 11 and 12 is particularly large, which is consistent with leaves 5 and 11 having the largest residuals from the best-fitting conformal map.

A.4. Fitting conformal maps

Conformal maps are fitted by least squares. For instance, a quadratic map $f(z) = a + bz + cz^2$, with $z = x + iy$, can be written in the form $f(z) = u(x, y) + iv(x, y)$, where

$$u(x, y) = a_0 + b_0x - b_1y + c_0(x^2 - y^2) - 2c_1xy,$$

and

$$v(x, y) = a_1 + b_0y + b_1x + c_1(x^2 - y^2) + 2c_0xy,$$

with $a = a_0 + ia_1$, $b = b_0 + ib_1$, $c = c_0 + ic_1$. then we find the values of a_0, a_1, b_0, b_1, c_0, c_1 that minimise the sum of squares error given by Eq. (A.5).

The Möbius transformation is fitted by writing the function $f(z) = (a + bz)/(c + dz)$ as a polynomial series, viz. $f(z) = (a/c + bz/c)\left(1 - dz/c + d^2z^2/c^2 - \ldots\right)$, and comparing its terms up to quadratic order with those of the best-fitting cubic. This determines a, b, c, d, up to an irrelevant shared factor. The cubic term in the expansion is then found to be quite closely approximated by that of the best-fitting cubic (which is in any case a very small term). In other words, the best-fitting cubic is already quite close to a Möbius transformation. This can be seen in the small changes in the residuals in Table A2.

A.5. Divergence and vorticity

Given any matrix $A = \begin{pmatrix} a & b \\ c & d \end{pmatrix}$, its determinant $\det A = ad - bc$ is the area of the parallelogram whose sides are the vectors from the origin to (a,c) and (b,d); this is because the determinant is the cross product of these two vectors. Equivalently, since these two vectors are the images of the vectors $(1, 0)$ and $(0, 1)$ under the linear map determined by A, $\det A$ is the ratio of the area after the map is applied to its initial value, so $\sqrt{\det A}$ is the linear change of scale under the map. Thus $\sqrt{\det A}$ gives the RG under the linear map A.

Given any map f: $(x, y) \to (u(x, y), v(x, y))$, not necessarily linear or conformal, the local linear map at a point is given by the Jacobian $J(f) = \begin{pmatrix} u_x & u_y \\ v_x & v_y \end{pmatrix}$ evaluated at that point, and consequently $\det J(f)$ is the RG at that point.

Now suppose we have a time-sequence of maps, f_t, beginning at $t=0$ with the identity map, $f_0(x, y) = (x, y)$. Then the relative growth *rate*, RGR_f, is defined to be the temporal derivative $RGR_f = d(RG_f)/dt$. We can write $f_\epsilon(x, y) = (x + \epsilon u(x, y), y + \epsilon v(x, y))$, where (u,v) is the velocity field following the position of points on the growing leaf. Then $J(f_\epsilon) = \begin{pmatrix} 1 + \epsilon u_x & \epsilon u_y \\ \epsilon v_x & 1 + \epsilon v_y \end{pmatrix}$, and up to first order in ϵ, $\sqrt{\det J(f_\epsilon)} \approx 1 + \frac{1}{2}(\epsilon u_x + \epsilon v_y)$. Thus $RGR_f = \frac{1}{2}(u_x + v_y) = \frac{1}{2}\nabla.(u, v)$, which is half the divergence of the velocity field.

This is the measure of RGR derived in Richards and Kavanagh (1943) and used in Erickson (1966), Silk and Erickson (1979) (though these authors dropped the factor of 1/2 and just used the divergence $\nabla.(u, v)$, as they were concerned with the areal rather than the linear RGR). They applied this measure to the velocity field based on successive observations 24 h apart. Since the leaf grew considerably between observations (20–40% length increase), the assumption of a small ϵ is not fully justified. The approach taken below (Appendices A.6 and A.8) is to interpolate the time sequence between observations and thus minimise this inaccuracy.

The vorticity is defined to be $\frac{1}{2}(v_x - u_y)$. We can understand this by combining the effect of a not necessarily isotropic expansion $\begin{pmatrix} g_1 & 0 \\ 0 & g_2 \end{pmatrix}$ and a rotation $\begin{pmatrix} \cos\theta, & -\sin\theta \\ \sin\theta, & \cos\theta \end{pmatrix}$ to give the map $A = \begin{pmatrix} g_1\cos\theta, & -g_1\sin\theta \\ g_2\sin\theta, & g_2\cos\theta \end{pmatrix}$. The vorticity is then $\frac{1}{2}(g_1 + g_2)\sin\theta$. For a short time interval, we can assume that g_1 and g_2 are ϵ-close to 1 and θ is of order ϵ, in which case the vorticity is approximately θ, and is independent of the expansion factors g_1 and g_2.

Thus for small time intervals, the divergence measures expansion and the vorticity measures the angle of rotation of the tissue. A simple example shows that this is not true for longer time intervals. Consider the map sending (x,y) to $(gy, -gx)$, i.e. the linear map $\begin{pmatrix} 0, & -g \\ g, & 0 \end{pmatrix}$. This corresponds to a 90 degree rotation combined with uniform expansion by a factor g. Yet its divergence is zero and its vorticity is g.

A.6. The relative growth rate of a family of conformal maps

We begin with an assumption, that is only an approximation to biological reality, that growth results from the repeated iteration of the same map that operates over a short time period. Thus we define the map $f_{1/n}$ to be the map whose n-fold composition is the map $f(z)$ observed over some time interval (e.g. the 24 h of the observations here). In other words,

$$f(z) = \underbrace{f_{1/n}(f_{1/n}(\ldots f_{1/n}(z)\ldots))}_{n}. \tag{A.8}$$

We assume that such a map $f_{1/n}$ exists for arbitrarily large n (i.e. arbitrarily short times). The reason this is not biologically fully plausible is that the map is likely to change as the leaf grows: what we are calling $f_{1/n}$ will not be quite the same map at the beginning and end of a sequence of iterations. However, the simplifying assumption makes the problem mathematically tractable, and is enshrined in the concept of a semigroup of maps, where $f_{s+t}(z) = f_s(f_t(z))$, for all positive s, t (Bracci et al., 2007). Henceforth we assume that $f_t(z)$, the map for a time period t, is defined for all t in some range $[0, T]$, i.e. for the duration of observations. We also assume that $f_t(z)$ is conformal for all t in this range, which is certainly true for the approximating functions (polynomials, Möbius transformations) that we use.

For a small time, $t = \epsilon$, the map $f_\epsilon(z)$ is close to the identity, and can therefore be written approximately as

$$f_\epsilon(z) \approx z + \epsilon g(z), \tag{A.9}$$

where $g(z)$ is called the *infinitesimal generator* of the semigroup (Bracci et al., 2007). Since $f_\epsilon(z)$ is conformal, so is the infinitesimal generator. As observed in Section A.5 above, $RGR_{f_t}(z) = \frac{1}{2}(h_x + k_y)$, where $g = h + ik$. From the Cauchy-Riemann equations, $h_x = k_y$, so we get

$$RGR_{f_t}(z) = h_x. \tag{A.10}$$

Now h_x, which is the real part of the analytic function $dg(z)/dz$, is harmonic. So the growth rate could be specified by the concentration of a substance at diffusive equilibrium. These steps can be reversed, since any harmonic function can be written as the real

part of some complex function $k(z)$ and we can take the conformal infinitesimal generator to be $g(z) = \int k(z)$. Since composition of conformal maps is conformal, the resulting growth is conformal. So specifying the growth rate by the concentration of a diffusible substance produces a conformal map. In the next section we outline Wolfram's very different argument that leads to the same conclusion.

A.7. Growth rates and curvature: Wolfram's argument

Instead of confining oneself to planar maps one can consider locally isotropic growth in the setting of curved surfaces. Suppose growth in an initially flat surface is isotropic, and that this growth gives rise to a curved surface. A rectangular coordinate system in the flat surface will be carried into a coordinate system $(u(x, y), v(x, y))$ that divides the surface into infinitesimal squares (see for example the tesselated 'Stanford bunny', Fig. 2.5 in Zeng and Gu, 2013). The coordinate system (u,v) is called an *isothermal* system, and the infinitesimal length element ds is given by $ds^2 = \lambda(du^2 + dv^2)$ (Struik, 1950), where $\lambda(x, y)$ is the isotropic local expansion. A well-known formula (Zeng and Gu, 2013, Eq. (2.13)) expresses the Gaussian curvature K of the surface as

$$K = -\frac{1}{\lambda^2}\nabla^2 \ln\lambda, \tag{A.11}$$

where ∇^2 is the Laplacian $\partial^2/\partial x^2 + \partial^2/\partial y^2$.

Wolfram (2002) assumes that growth is locally isotropic, invokes a version of Eq. (A.11), and observes that if $K=0$, so the surface remains flat, then $\nabla^2 \ln\lambda = 0$. He interprets $\ln\lambda$ as the RGR and deduces that it must be a harmonic function. It is not clear why $\ln\lambda$ should be the RGR in general. However, in the case where λ is a function of time, assuming we can write $\lambda \approx \exp(\rho t)$ for small t, then ρ is indeed the RGR and the time derivative of Eq. (A.11) with $K=0$ gives $\nabla^2\rho = 0$.

The connection with curvature given by Eq. (A.11) is intriguing, and suggests mechanisms, perhaps combining reaction and diffusion, for generating curved surfaces.

A.8. The relative growth rate of a Möbius transformation family

Calculating the infinitesimal generator is easy for a Möbius transformation f. If A is the matrix representing f for a time interval which we take to be $t=0$ to $t=1$, then A^t, i.e. A raised to the power t, is the matrix representing f_t (see Fig. 9 for an illustration of $f_{1/2}$). In the limit of small ϵ,

$$A^\epsilon \approx \mathrm{id} + \epsilon \log A, \tag{A.12}$$

where $\log A$ is the matrix logarithm of A. Writing

$$\log A = \begin{pmatrix} b & a \\ d & c \end{pmatrix}, \tag{A.13}$$

and converting the matrix A^ϵ back into a Möbius transformation gives (neglecting terms in ϵ^2 or higher powers)

$$f_\epsilon(z) \approx \left[\epsilon a + (1+\epsilon b)z\right]\left[(1-\epsilon c) - \epsilon d z\right] \approx z + \epsilon g(z), \tag{A.14}$$

where

$$g(z) = a + (b-c)z - dz^2. \tag{A.15}$$

Thus the infinitesimal generator $g(z)$ is a quadratic polynomial. Eq. (A.10) now gives

$$\begin{aligned} RGR_f(z) = h_x(z) &= \Re\left[\frac{g(z)}{dz}\right] = \Re[(b-c) - 2dz] \\ &= (b_0 - c_0) - 2d_0 x - 2d_1 y, \end{aligned} \tag{A.16}$$

where b, c, d are the entries in $\log A$ defined above with $b = b_0 + ib_1$, $c = c_0 + ic_1$, $d = d_0 + id_1$. Thus three real parameters are needed to define the growth.

A.9. Powers and logs of matrices

The square root $\sqrt{F}$ of a matrix F is defined by the property that $(\sqrt{F})^2 = F$. If F can be diagonalized (as will be the case for those matrices considered in this paper), then we can write $F = P\begin{pmatrix} \lambda & 0 \\ 0 & \mu \end{pmatrix}P^{-1}$, for some invertible matrix P and eigenvalues λ and μ, and then $\sqrt{F}$ is defined by $\sqrt{F} = P\begin{pmatrix} \sqrt{\lambda} & 0 \\ 0 & \sqrt{\mu} \end{pmatrix}P^{-1}$. For 2×2 matrices, there are in general four choices of square root corresponding to the four choices of sign for $\sqrt{\lambda}$ and $\sqrt{\mu}$. In the applications here we use the principal value of the square roots, which is also the value provided by Matlab's matrix square root function. There is also a simple formula for calculating the square root of a 2×2 matrix which does not require diagonalising the matrix; see Sullivan (1993).

Other functions of matrices are defined similarly. Thus, given some function ϕ, such as an exponential, logarithm or any power, and given $F = P\begin{pmatrix} \lambda & 0 \\ 0 & \mu \end{pmatrix}P^{-1}$, we define $\phi(F) = P\begin{pmatrix} \phi(\lambda) & 0 \\ 0 & \phi(\mu) \end{pmatrix}P^{-1}$.

References

Arnold, D., Rogness, J., 2008. Mobius transformations revealed. Not. Am. Math. Soc. 55 (10), 1226–1231.

Avery, G., 1933. Structure and development of the tobacco leaf. Am. J. Bot. 20 (9), 565–592.

Bilsborough, G., Runions, A., Barkoulas, M., Jenkins, H., Hasson, A., Galinha, C., Laufs, P., Hay, A., Prusinkiewicz, P., Tsiantis, M., 2011. Model for the regulation of Arabidopsis thaliana leaf margin development. Proc. Nat. Acad. Sci. USA 108 (8), 3424–3429. http://dx.doi.org/10.1073/pnas.1015162108.

Bracci, F., Contreras, M., Diaz-Madrigal, S., 2007. Infinitesimal generators associated with semigroups of linear fractional maps. J. D.'Anal. Math. 102, 119–142. http://dx.doi.org/10.1007/s11854-007-0018-9.

Crank, J., 1975. The Mathematics of Diffusion. Clarendon Press, Oxford.

Cui, M.-.L., Copsey, L., Green, A., Bangham, J., Coen, E., 2010. Quantitative control of organ shape by combinatorial gene activity. PLoS Biol. 8 (11), e1000538. http://dx.doi.org/10.1371/journal.pbio.1000538.

Driever, W., Nüsslein-Volhard, C., 1988. A gradient of bicoid protein in drosophila embryos. Cell 54, 83–93.

Driever, W., Nüsslein-Volhard, C., 1988. The bicoid protein determines position in the drosophila embryo in a concentration-dependent manner. Cell 54, 95–104. http://dx.doi.org/10.1016/0092–8674(88)90183-3.

Engelhorn, J., Reimer, J., Leuz, I., Gobel, U., Huettel, B., Farrona, S., Turck, F., 2012. Development-related pcg target in the apex 4 controls leaf margin architecture in Arabidopsis thaliana. Development 139, 2566–2575. http://dx.doi.org/10.1242/dev.078618.

Erickson, R., 1966. Relative elemental rates and anisotropy of growth in area: a computer programme. J. Exp. Bot. 17 (51), 390–403.

Goebel, K., 1905. The Organography of Plants (English Translation). Clarendon Press, Oxford.

Green, A., Kennaway, J., Hanna, A., Bangham, J., Coen, E., 2010. Genetic control of organ shape and tissue polarity. PLoS Biol. 8 (11), 1000537. http://dx.doi.org/10.1371/journal.pbio.1000537.

Gregor, T., Tank, D., Wieschaus, E., Bialek, W., 2007. Probing the limits to positional information. Cell 130, 153–164. http://dx.doi.org/10.1016/j.cell.2007.05.025.

Jones, G., Mahadevan, L., 2013. Planar morphometry, shear and optimal quasi-conformal mappings. Proc. R. Soc. A 469, 20120653. http://dx.doi.org/10.1098/rspa.2012.0653.

Kennaway, R., Coen, E., Green, A., Bangham, J., 2011. Generation of diverse biological forms through combinatorial interactions between tissue polarity and growth. PLoS Comput. Biol. 7 (6), e1002071. http://dx.doi.org/10.1371/journal.pcbi.1002071.

Kuchen, E., Fox, S., de Reuille, P.B., Kennaway, R., Bensmihen, S., Avondo, J., Calder, G., Southam, R., Robinson, S., Bangham, A., Coen, E., 2012. Generation of leaf shape through early patterns of growth and tissue polarity. Science 335, 1092–1096. http://dx.doi.org/10.1126/science.1214678.

Lawrence, P., 1966. Gradients in the insect segment: the orientation of hairs in the milkweed bug Oncopeltus fasciatus. J. Exp. Biol. 44, 607–620.

Liang, H., Mahadevan, L., 2011. Growth, geometry, and mechanics of a blooming lily. PNAS 108 (14), 5516–5521. http://dx.doi.org/10.1073/pnas.1007808108.

Mahadevan, L., Liang, H., 2009. The shape of a long leaf. PNAS 106 (52), 22049–22054. http://dx.doi.org/10.1073/pnas.0911954106.

Needham, T., 1997. Visual Complex Analysis. Clarendon Press, Oxford.

Remmler, L., Rolland-Lagan, A.-G., 2012. Computational method for quantifying growth patterns at the adaxial leaf surface in three dimensions. Plant Physiol. 159, 27–39. http://dx.doi.org/10.1104/pp.112.194662.
Richards, O., Kavanagh, A., 1943. The analysis of the relative growth gradients and changing form of growing organisms: illustrated by the tobacco leaf. Am. Nat. 77, 385–399.
Rolland-Lagan, A.-G., Bangham, J., Coen, E., 2003. Growth dynamics underlying petal shape and asymmetry. Nature 422, 161–163. http://dx.doi.org/10.1038/nature01443.
Rolland-Lagan, A.-G., Remmler, L., Girard-Bock, C., 2014. Quantifying shape changes and tissue deformation in leaf development. Plant Physiol. 165, 496–505. http://dx.doi.org/10.1104/pp.113.231258.
Sauret-Gueto, S., Schiessl, K., Bangham, A., Sablowski, R., Coen, E., 2013. Jagged controls arabidopsis petal growth and shape by interacting with a divergent polarity field. PLoS Biol. 11, e1001550. http://dx.doi.org/10.1371/journal.pbio.1001550.
Schwartz, E., 1977. The development of specific visual connections in the monkey and the goldfish: outline of a geometric theory of receptotopic structure. J. Theor. Biol. 69, 655–683.
Silk, W., Erickson, R., 1979. Kinematics of plant growth. J. Theor. Biol. 76, 481–501.
Struik, D., 1950. Lectures on Classical Differential Geometry. Addison-Wesley Reading, Massachusetts, USA, London, England.
Sullivan, D., 1993. The square roots of 2×2 matrices. Math. Mag. 66 (5), 314–316. http://dx.doi.org/10.2307/2690509.
Thompson, D.W., 1917. On growth and Form. Cambridge University Press, Cambridge, England.
Wolfram, S., 2002. A New Kind of Science. Wolfram Media Inc, Champaign, Illinois.
Wolpert, L., 1969. Positional information and the spatial pattern of cellular differentiation. J. Theor. Biol. 25 (1), 1–47. http://dx.doi.org/10.1016/S0022-5193(69)80016-0.
Zeng, W., Gu, X., 2013. Ricci Flow for Shape Analysis and Surface Representation: Theories, Algorithms and Applications. Springer, New York, Heidelberg, Dordrecht, London.